Measurement of the cross sections for electron-impact excitation into the $5p^5 6p$ levels of xenon

John T. Fons and Chun C. Lin
Department of Physics, University of Wisconsin, Madison, Wisconsin 53706
(Received 22 June 1998)

Electron-impact emission cross sections for transitions from the ten $5p^5 6p$ levels of xenon to the lower levels have been measured at different gas pressures between 0.1 and 2.0 m Torr, and with incident electron energy from threshold to 150 eV. The exceptionally strong pressure dependence of the measured emission cross sections reported previously is confirmed. The optical emission cross sections yield the apparent excitation cross sections for the $5p^5 6p$ levels which vary significantly with pressure. Use of a Fourier-transform spectrometer makes it possible to measure previously uninvestigated infrared cascade transitions into the $5p^5 6p$ levels. Our measured cascade cross sections increase with pressure because of radiation trapping effects, and their pressure dependence is similar to that of the apparent excitation cross sections. By subtracting the cascade contribution from the apparent cross sections, we obtain the direct excitation cross sections which are found to be independent of the pressure. The peak direct cross sections for the $2p_1$-$2p_4$ levels (Paschen's notation) are much smaller than those of the $2p_5$-$2p_{10}$ group. This is explained on the basis that the ionization energies for the former group are about only one-half of those for the latter group. Within each of these two groups ($2p_1$-$2p_4$ and $2p_5$-$2p_{10}$), the levels with even values of the total angular momentum J have larger cross sections than the levels with odd J. [S1050-2947(98)08312-7]

PACS number(s): 34.80.Dp, 34.80.My

I. INTRODUCTION

Electron-impact excitation cross-section measurements on the rare gases have been increasingly important in laser, lighting, and plasma technologies. Early measurements of xenon by Fel'stan and Zapesochnyi [1] and by Rostovikova, Samoilov, and Smirnov [2] covered optical emission cross sections for over 30 transitions, but the two sets of cross sections are not always in good agreement. An exceptionally strong pressure dependence of the measured optical cross sections for emission from the $5p^5 6p$ levels was later reported by Walker [3], and subsequently confirmed in other laboratories [4,5]. This effect was shown in some cases to persist at pressures down to 0.1 m Torr. The origin of this pressure dependence has been thought to be collisional excitation transfer or radiation trapping, which causes certain emission rates to increase with pressure, but there was no experimental verification. Such pressure-dependent emission cross sections are difficult to interpret, and are of limited use unless the origin of the observed pressure effects is understood.

Another complication in the study of electron excitation of xenon is that a large part of the emission lines is in the infrared, outside the range of detection of the photomultiplier tubes (PMT's) traditionally used in the optical measurements. The lack of emission cross-section data in the infrared region had greatly impeded the study of cascade population of some levels (such as $5p^5 6p$), and the direct excitation of others (such as $5p^5 5d$). This limitation, however, has been overcome by the work of DeJoseph and Clark in which they pioneered the use of Fourier-transform spectroscopy (FTS) for the detection of the infrared radiation emitted in electron-impact experiments [5]. They reported optical emission cross sections for a number of $5p^5 5d \rightarrow 5p^5 6p$ transitions ($3d \rightarrow 2p$ in Paschen's notation) at wavelengths as high as 3996 nm.

Pressure dependence of the optical emission cross sections was previously observed for other rare gases, although the effects are not as prominent and extensive as in Xe. The $3\,^1P \rightarrow 2\,^1S$ emission cross section of He shows a pressure dependence down to pressures as low as 0.8 m Torr [6]. This is due to reabsorption of the $3\,^1P \rightarrow 1\,^1S$ resonant emission by nearby ground-state He atoms. As the He($3\,^1P$) atoms, resulting from reabsorption, decay through the $2\,^1S$ channel, we see an enhancement of the $3\,^1P \rightarrow 2\,^1S$ emission. The number of emission-reabsorption cycles increases at higher pressure so that the $3\,^1P \rightarrow 2\,^1S$ enhancement becomes proportionally larger. A somewhat different version of the pressure effect was seen in argon, in which the emission cross sections of some of the $3p^5 4p \rightarrow 3p^5 4s$ transitions ($2p \rightarrow 1s$ in Paschen's notation) increase by over a factor of 2 from 0.5 to 4.0 m Torr. Here the $3p^5 4p$ levels are not affected by radiation trapping, since they are not optically connected to the $3p^6$ ground state. If the $3p^5 4p$ levels were populated entirely by direct electron-impact excitation, the radiation from these levels should not show the kind of pressure dependence described above. However, the $3p^5 4p$ levels are also populated by cascade from the $3p^5 nd$ and $3p^5 ns$ levels, some of which are optically coupled to the ground state and therefore subject to radiation trapping. Through radiative cascade, the pressure effects of these optically allowed levels propagate to the $3p^5 4p$ levels. To examine this point, Chilton *et al.* [7] recently performed a systematic study of the pressure effect on the excitation of the $3p^5 4p$ levels of argon, in which they measured the optical emission cross sections for the infrared cascade radiation from the $3p^5 5s$ and $3p^5 3d$ levels into the ten $3p^5 4p$ levels of argon using the FTS technique. The total cascade into each $3p^5 4p$ level was found to exhibit the same pressure dependence as the apparent excitation cross section of that level, so that when the cascade is subtracted from the apparent excitation cross section, the resulting direct excitation cross sections are

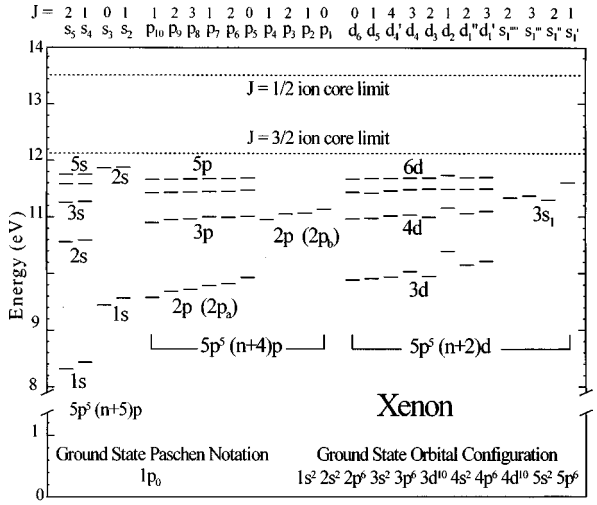

FIG. 1. The energy-level diagram for the xenon atom (in units of eV). The top of the figure lists the J value followed by Paschen's notation for each level. Conversion to configuration is provided at the bottom, where n is the numerical prefix in Paschen's notation. The ionization limits for the formation of the $5p^5(^2P_{3/2})$ and $5p^5(^2P_{1/2})$ cores are indicated by dashed lines.

independent of the target gas pressure from 0.5 to 4.0 m Torr. Thus the observed pressure dependence in the emission cross section of the $3p^5 4p \rightarrow 3p^5 4s$ transitions of argon is attributed entirely to radiation trapping through cascade population.

In this paper, we undertake a systematic study of the optical cross sections for the emissions from the $5p^5 6p$ levels of the Xe atom, with emphasis on their pressure dependence. In Fig. 1 we show an energy-level diagram for Xe. Emission cross sections for cascade radiation into the $5p^5 6p$ levels from the higher configurations, $5p^5 ns$ and $5p^5 nd$, are measured over a wide range of pressure. Optical detection is made by a FTS as well as a monochromator-PMT system to cover the wavelength range of 200–5000 nm. These measurements enable us to determine the origin of the observed pressure dependence of the emission cross sections. We have also obtained the direct excitation cross sections for the ten levels of the $5p^5 6p$ configuration, and found a significant difference in the general trend as compared to the lighter rare gases.

II. EXPERIMENT

The apparatuses shown in Figs. 2 and 3 were used to measure the electron-impact excitation cross sections through optical detection by means of PMT's and FTS, respectively. Details of the apparatuses and processes are available in the literature [8,9], so only a brief description will be given here. For both experimental setups, a monoenergetic electron beam is formed by electrostatically accelerating and focusing electrons produced by an indirectly heated BaO cathode. The electron beam has a diameter of 3 mm and covers an energy range of 10–150 eV with a typical energy spread of 0.5 eV full width at half maximum (FWHM). We find that the buildup of contaminants in the collision chamber over a long period of time begins to affect the energy of the electron beam, and that the true kinetic

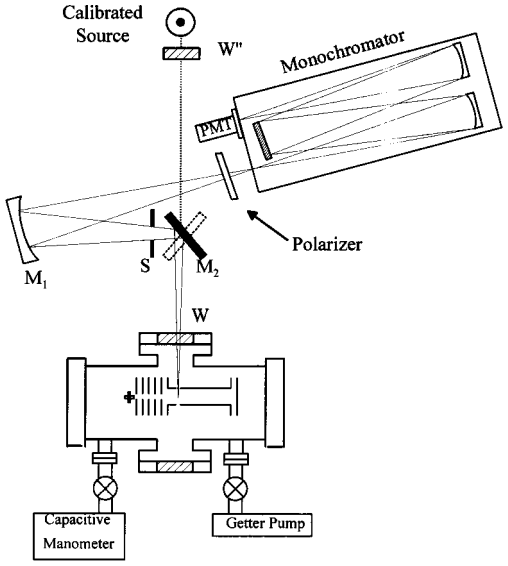

FIG. 2. Monochoromator-PMT system used for absolute cross-section determination.

energy of the electrons is not necessarily equal to the accelerating potential. The energy difference between the actual electron energy and the applied voltage is known as the energy offset, and was regularly monitored to be approximately 5 eV, with a variation of about 5% over a period of several months. We determined the energy offset by increasing the energy of the electron beam until the optical emission from the excited level of our interest was observed. At this point, the energy offset is equal to the difference between the accelerating voltage and the energy threshold of excitation [8,9]. We have used emission lines from various excited states over a wide range of intensity to determine the energy offset, and the results are consistent within the variation cited above. All measurements reported here have been corrected to compensate for this energy offset.

Figure 2 shows the apparatus in which a monochromator is used for optical detection. A combination of ion, getter, diffusion, and mechanical pumps is used to evacuate the chamber to approximately 5×10^{-8} Torr. The chamber is then filled with Xe gas to the desired pressure, 0.1–2.0 m Torr, which is continuously monitored by a 0.1-Torr ca-

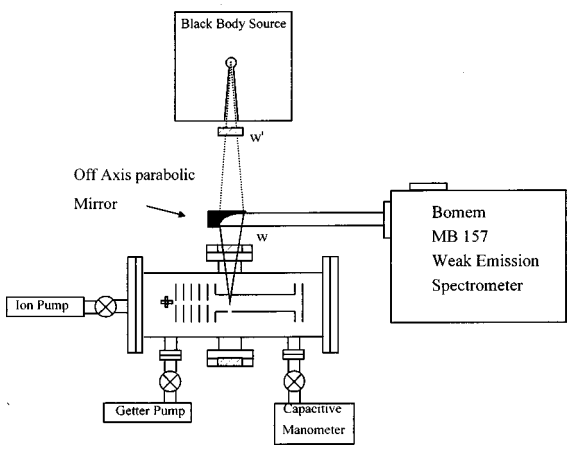

FIG. 3. Fourier-transform spectrometer system used for relative cross-section measurement.

pacitive manometer. The electron beam is monitored by an electrometer, and the results are read by computer for analysis. The emissions from the collision chamber are reflected off mirror M1 and are focused by mirror M2 onto the entrance slits of a 1.26 m Czerny-Turner monochromator. A PMT at the exit slit of the monochromator is used to detect the radiation. By rotating the monochromator grating, a plot of the intensity of the radiation as a function of the wavelength is created. The exit and entrance slits of the monochromator were typically set to give a resolution of 1.25-Å FWHM. Two types of PMT's were used for these studies. A high sensitivity, low noise Burle PMT, model 31034, with a GaAs photocathode, was used in the wavelength range from 200 up to about 890 nm. A Hamamatsu PMT with a *S*1 photocathode, model *R*1767, was used from approximately 800 to 1050 nm. To dramatically reduce the amount of dark current, both these PMTs have been cooled. The GaAs PMT was thermoelectrically cooled to -30 °C and, the *S*1 PMT was cooled to -60 °C with a liquid-nitrogen system. Rotating the plane mirror M1 by 90° reflects the radiation from a calibrated standard lamp and allows it to travel along the same optical path. Doing so allows for compensation of the optical efficiencies of all the components and we can then determine the absolute emission intensity of the radiation from the collision chamber. The quartz window W' was introduced into the optical path of the standard lamp to compensate for the transmission characteristics of the window W on the chamber. A tungsten halogen lamp was used in the wavelength range of 400–1100 nm, and a deuterium lamp was used in the 200–400-nm region for calibration purposes. Both of these standard lamps were calibrated by the manufacturer. By making a plot of absolute intensity versus wavelength and measuring the area under the curve, we can determine the absolute emission cross section for a given transition. The optical emission cross section for the $j \rightarrow k$ transition, Q_{jk}^{opt}, is defined as

$$Q_{jk}^{\mathrm{opt}} \equiv \frac{\Phi_{jk}}{n_0(I/e)}, \tag{1}$$

where Φ_{jk} is the number of photons per unit beam length emitted in the $j \rightarrow k$ transition, I is the electron-beam current, n_0 is the number density of the ground-state atoms, and e is the magnitude of the electron charge.

To check the polarization of the emission cross sections, a polarizer was placed in the optical path, as shown in Fig. 2. Since the grating shows a significant difference in the reflection efficiency for parallel and perpendicularly polarized radiation, the standard lamp is used to determine the relative efficiency for the two polarizations.

The PMT systems have been used in a photon-counting mode as well as an analog mode. When photon counting, the output from the PMT is sent through a series of amplifiers where it is then fed through a discriminator and a photon counter. To remove the background radiation, the electron beam is electronically gated at a frequency of 1 kHz. While the electron beam is on, the photon counter detects the photons emitted from the collision chamber, the scattered radiation from the heated cathode, and the dark counts arising from the PMT itself. While the electron beam is off, the detector determines the amount of scattered background radiation and dark current. By subtracting the two results, we are able to isolate the signal from the background. Approximately 5×10^4 to 10^6 gate pairs are used to determine the signal at a given wavelength, electron-beam energy, pressure, and electron-beam current.

The apparatus shown in Fig. 2 has also been used in an analog mode. Here, the current from the PMT is sent directly into an electrometer whose output is then recorded by the computer. When sweeping the monochromator over long portions of the spectra, hundreds of nm, we have found that when the emission intensity is sufficient, using the analog mode is more time efficient than using the photon-counting mode. This analog process was used for relative cross-section determination and general spectral investigations. While utilizing this analog method, the electron beam is not gated and the background was removed graphically. Photon counting was used exclusively in all other studies, including current and pressure dependence, as well as excitation functions and absolute calibration procedures.

The apparatus shown in Fig. 3 utilizes a Bomem Model MB 157 FTS system for the infrared emission studies. Here, the emissions from the collision chamber are collimated and sent into the entrance port of the spectrometer. 50–500 individual interferograms were averaged together, and were converted into an intensity versus wavelength plot through the use of the Fourier transform function. The advantage of the FTS system over the PMT systems is that even a single run gives information about the complete spectrum instead of just a very narrow segment. By rotating the collimating mirror 180°, the emissions from a blackbody source can follow the same optical path, so that the relative efficiency of the optics and detector as a function of the wavelength can be made. For this apparatus, we again introduce a window W' to compensate for the transmission characteristics of the CaF_2 window on the chamber, W. Knowing the relative efficiencies allows for the determination of the relative intensities and relative cross sections of the emissions contained in the spectrum.

Two different types of photodiodes have been used with the FTS system, the first being a 0.5-mm $In_xGa_{1-x}As$ detector cooled to -30 °C to reduce noise. When cooled, this detector has a manufacturers specified wavelength range of 910–1610 nm, although, by heating it to approximately 50 °C, we can increase its wavelength range to about 1750 nm. This was done to extend its range to allow for the detection of the $3d_2$-$2p_9$ transition at 1733 nm. The other type of detector used is a 1-mm InSb photodiode that was cooled to 77 K. Two different InSb detectors have been used, one with a filter that passes 1300–2800-nm light, and another that has no filter and can be used out to approximately 5500 nm. The purpose of the filter is to reduce the blackbody radiation at the longer wavelengths, which allows for greater amplification of the remaining spectral range. The sensitivities of the InSb detectors are much poorer than that of the $In_xGa_{1-x}As$ detector, so, whenever possible, the $In_xGa_{1-x}As$ detector was used. The blackbody source used to calibrate the relative efficiencies of the FTS system was heated to 1050 and 850 °C for the $In_xGa_{1-x}As$ and InSb detectors respectively.

While using FTS, the pressure of the xenon gas was again monitored by a capacitive manometer. The electron beam

TABLE I. Emission cross sections (in units of 10^{-20} cm^2) for transitions out of the $2p$ levels at an electron energy of 30 eV and a pressure of 1.0 mTorr. The values in parentheses next to the level are the J value for that level. The ellipses represent emissions too weak to reliably measure, typically less than 5×10^{-20} cm^2. Entries with an X correspond to forbidden transitions. Cross sections in parentheses were determined by theoretical branching ratios and measured cross sections out of the same upper level (see text); no uncertainty limits are given for these values. Blank entries represent energetically impossible transitions. The last row corresponds to the apparent cross section for a given $2p$ level.

	$2p_1$ (0)	$2p_2$ (1)	$2p_3$ (2)	$2p_4$ (1)	$2p_5$ (0)	$2p_6$ (2)	$2p_7$ (1)	$2p_8$ (3)	$2p_9$ (2)	$2p_{10}$ (1)
$1s_2$ (1)	340±51	21.8±3.3	265±40	35.0±5.1	(4.1)	(0.53)	⋯	X	⋯	⋯
$1s_3$ (0)	X	35.4±5.3	X	34.5±5.3	X	X	⋯	X	X	⋯
$1s_4$ (1)	16.7±3.4	⋯	5.8±1.7	7.5±2.1	1924±288	194±29.5	965±145	X	969±147	12.5±2.1
$1s_5$ (2)	X	⋯	9.7±2.3	⋯	X	593±89.0	106±16.2	615±93	592±89	517±76
$2s_4$ (1)	(23.8)	(0.6)	⋯	(3.1)						
$2s_5$ (2)	X	(2.5)	(6.1)	(2.7)						
$3d_1'$ (3)	X	X	4.7±0.85	X						
$3d_1''$ (2)	X	⋯	⋯	⋯						
$3d_2$ (1)	(10.3)	⋯	(0.34)	(0.74)						
$3d_3$ (2)	X	⋯	⋯	⋯						
$3d_4$ (3)	X	X	⋯	X						
$3d_5$ (1)	82.1±14.0	3.7±0.72	15.5±2.6	⋯	⋯					
$3d_6$ (0)	X	6.9±1.4	X	⋯	⋯					
Total	473±60.8	70.9±8.5	307±43.3	83.5±9.6	1928±288	798±94.6	1071±146	615±93	1561±152	530±78

was not gated in this case, and was continuously measured by a digital ammeter. Over the duration of one investigation, 2–20 min, the pressure and current did not change by more than 1%.

Since FTS is capable of determining only relative cross sections, it is important that there be some overlap region in the wavelength ranges of the various detectors. The $2p_9 \rightarrow 1s_4$ and $2p_{10}\rightarrow 1s_5$ emissions can be readily measured with the Hamamatsu PMT and the $In_xGa_{1-x}As$ detector. We use these cross sections to put all other cross sections in the $In_xGa_{1-x}As$ spectrum on an absolute scale. Likewise, we then use the $2s_4\rightarrow 2p_7$ transition at 1542 nm to put the results of the InSb detector measurements on an absolute scale relative to the same transition measured by the $In_xGa_{1-x}As$ detector.

For both apparatuses, the dependence of the emission cross sections on the pressure and the electron-beam energy has been investigated. To determine the cross-section dependence on the pressure, we held the electron-beam energy constant, and changed the pressure while monitoring the current. The cross-section dependence on the energy, or excitation function, is determined by holding the pressure constant and changing the energy of the electron beam while monitoring the beam current. The pressure range was 0.1–2.0 mTorr and the energy ranged from 5 up to 150 eV. Throughout the investigations, the beam current was typically between 10 and 250 μA, although because of their relatively poor sensitivity, higher beam currents ~500 μA were used with the InSb detectors. The lower currents were used because of an increased stability in the magnitude and shape of the electron beam. To verify that the cross sections were linear with current over these ranges, we held the energy and pressure constant while changing the beam current. Adjusting the voltages on the electron gun grids in order to increase the current could cause an unwanted change in the beam shape or energy offset. Instead, we adjusted the current by altering the BaO cathode temperature. To within 3%, we find the cross section to be linear with current up to a current of 600 μA.

III. RESULTS

The optical emission cross sections for transitions out of the ten $2p$ levels are given in Table I for an electron-beam energy of 30 eV and a pressure of 1.0 m Torr. By summing over all emission cross sections out of a given $2p$ level into all lower levels, we can determine the apparent cross section for the $2p$ level,

$$Q_j^{\mathrm{app}}=\sum_{k<j} Q_{jk}^{\mathrm{opt}}. \tag{2}$$

The apparent cross sections for the $2p$ levels are given in the last row of Table I. In several cases the emissions cross sections were not measured directly because the wavelength of the transition was outside the ranges of the various detectors or there was a significant absorption of the radiation due to water vapor or carbon dioxide in the atmosphere. For these transitions $(i\rightarrow n)$ the cross sections were obtained by measuring the cross sections for another transition from the same upper level $(i\rightarrow m)$, and utilizing the relation

$$Q_{\mathrm{in}}^{\mathrm{opt}}=\frac{A^{\mathrm{th}}(i\rightarrow n)}{A^{\mathrm{th}}(i\rightarrow m)}\,Q_{\mathrm{im}}^{\mathrm{opt}}, \tag{3}$$

where the A^{th}'s are the transition probabilities obtained by theoretical calculations [10] using Hartree-Fock wave functions with intermediate coupling. Because of the difficulty of treating an atom as complex as Xe theoretically, Eq. (3) is used only as a means to estimate the unmeasured cross sections. These estimated cross sections are designated by parentheses in Table I. They are generally quite small com-

TABLE II. Optical emission cross sections for transitions into the $2p$ manifold from higher levels for an electron-beam energy of 30 eV and a pressure of 1.0 mTorr. The first column corresponds to the upper level (with the J value in parentheses). Entries of X correspond to optically forbidden transitions. Entries in parentheses correspond to cross sections determined by theoretical branching ratios and measured cross sections out of the same upper level (see text). Ellipses represent cross sections which are insignificant compared to the corresponding direct cross section of the $2p$ level (Table III). Blank entries correspond to transitions which are energetically impossible. The row labelled as ''Other'' is a sum of all cascade cross sections not individually listed. The total uncertainty (systematic and statistical) in the individual cross sections is generally between 15 and 22%.

	$2p_1$ (0)	$2p_2$ (1)	$2p_3$ (2)	$2p_4$ (1)	$2p_5$ (0)	$2p_6$ (2)	$2p_7$ (1)	$2p_8$ (3)	$2p_9$ (2)	$2p_{10}$ (1)
$2s_2$ (1)	(13.1)	15.4	40.8	⋯	⋯	⋯	8.2	X	⋯	25.2
$2s_3$ (0)		⋯		⋯	X	X	⋯	X	X	113
$2s_4$ (1)					(26.2)	26.6	148	X	197	15.8
$2s_5$ (2)					X	⋯	⋯	18.8	⋯	23.5
$3d_2$ (1)					51	⋯	199	X	153	⋯
$3s_1'$ (1)	(19.0)	12.7	6.3	24.1	9.6	⋯	17.1	X	3.5	11.9
$3s_1'''$ (3)	X	X	(66.4)	X	X	5.5	X	28.8	75.3	X
$3s_1''''$ (2)	X	⋯	⋯	⋯	X	25.0	⋯	35.1	⋯	⋯
$3s_4$ (1)	⋯	⋯	⋯	⋯	⋯	⋯	⋯	X	32.7	5.2
$3s_5$ (2)	X	⋯	⋯	⋯	X	⋯	⋯	18.4	4.7	13.9
$4d_1'$ (3)		X	⋯	X	X	133	X	⋯	⋯	X
$4d_1''$ (2)			⋯	*(26.4)*	X	⋯	⋯	165	⋯	⋯
$4d_2$ (1)	⋯	⋯	⋯	*(6.4)*	241	⋯	105	X	7.8	⋯
$4d_3$ (2)				X	X	⋯	⋯	⋯	47.8	⋯
$4d_4$ (3)				X	X	⋯	X	15.5	36.5	X
$4d_4'$ (4)				X	X	X	X	45.6	X	X
$5d_2$ (1)	⋯	⋯	⋯	⋯	74	⋯	⋯	X	3.9	⋯
$5d_4$ (3)	X	X	⋯	X	X	8.2	X	5.1	75.1	X
$5d_4'$ (4)	X	X	X	X	X	X	X	31.6	X	X
$5d_5$ (1)	⋯	⋯	⋯	⋯	3.0	7.1	⋯	X	⋯	40.5
$5s_4$ (1)	⋯	⋯	⋯	⋯	⋯	⋯	11.7	X	⋯	8.3
$6d_1'$ (3)	X	X	⋯	X	X	18.5	X	⋯	⋯	X
$6d_2$ (1)	⋯	⋯	⋯	⋯	51.7	⋯	38.9	X	⋯	⋯
$6d_4$ (3)	X	X	⋯	X	X	⋯	X	2.1	25.0	X
$6d_5$ (1)	⋯	⋯	⋯	⋯	⋯	2.9	3.7	X	3.4	21.1
$6s_5$ (2)	X	⋯	⋯	⋯	X	⋯	⋯	31.7	⋯	⋯
$7d_2$ (1)	⋯	⋯	⋯	⋯	37.2	⋯	22.3	X	10.0	2.7
Other	7.3	0	2.7	3.5	2.1	18.4	20.7	15.7	9.0	29.4
Total	39.4±5.7	28.1±5.0	116±18.5	60.4±10	496±80	245±44.8	575±92.0	413±64.8	685±103	311±46.8

pared to the cross sections that were measured directly, and individually constituted no more than 5% of the corresponding apparent excitation cross sections.

Polarization of emissions for the apparent cross sections has been measured. We have found that the radiation emitted from the collision region generally shows a polarization less than 7%, so the polarization correction to the cross sections amounts to about only 2%.

We must recall that there are two main ways to populate the various $2p$ levels in the basic electron collision experiment. First we have direct excitation due to electron impact with a ground-state atom. The second method is a result of radiative cascade into the $2p$ levels from higher-lying levels (*ns* and *nd*) excited by the electron beam. We have measured the individual emission cross sections for the cascade transitions from the *ns* and *nd* manifolds with *n* values (the numerical prefix in Paschen's notation) as large as 7. Table II shows the cross sections for all the transitions into the $2p$ levels of xenon for an electron energy of 30 eV. Cascade emission cross sections less than 5% of the apparent cross section are not listed individually, but are summed together and listed as ''Other'' in Table II.

The total cascade contribution to the apparent cross section of the level j is obtainable by summing over all optical emission cross sections from the higher-lying levels,

$$Q_j^{\mathrm{cas}} = \sum_{i>j} Q_{ij}^{\mathrm{opt}}. \tag{4}$$

The direct excitation cross section Q^{dir} is then found from the experimentally measured quantities as

$$Q_j^{\mathrm{dir}} = Q_j^{\mathrm{app}} - Q_j^{\mathrm{cas}}. \tag{5}$$

Included in Table II are the total cascade contribution for each $2p$ level at 30 eV which is to be subtracted from the corresponding apparent cross section to give the direct excitation cross sections, as shown in Table III.

TABLE III. Apparent, cascade, and direct cross sections (in units of 10^{-20} cm^2) for an electron-beam energy of 30 eV and pressure of 1.0 mTorr. The value in parentheses next to the level is the J value for that level. The uncertainties given represent the total uncertainty in the cross sections.

	$2p_1$ (0)	$2p_2$ (1)	$2p_3$ (2)	$2p_4$ (1)	$2p_5$ (0)	$2p_6$ (2)	$2p_7$ (1)	$2p_8$ (3)	$2p_9$ (2)	$2p_{10}$ (1)
Apparent	473±60.8	70.9±8.5	307±43.3	83.5±10.9	1928±288	788±94.6	1071±146	615±93.0	1561±152	530±78
Cascade	39.4±5.7	28.1±5.0	116±18.5	60.4±10	496±80	245±44.8	575±92.0	413±64.8	685±103	311±46.8
Direct	434±61.8	42.8±10.2	191±53	23.1±15.5	1432±302	543±109	496±180	202±116	876±189	219±93

To study the effect of gas pressure, the emission cross sections at 30 eV are remeasured at several different pressures between 0.1 and 2.0 m Torr. For illustration, in Fig. 4 we show the pressure dependence of the cross sections for emission from the $2p_7$, $3s_4$ ($5p\,^5 8s$, $J=1$), and $3d_2$ ($5p\,^5 5d$, $J=1$) levels. For the most severe case of $3d_2$, the cross section appears to increase by a factor of 30 from 0.1 to 2.0 m Torr.

From the emission cross sections taken at different pressures for the transitions listed in Tables I and II, we obtain the pressure dependence of the apparent excitation cross sections and the cascade cross sections for the ten $2p$ levels. Figure 5 shows these cross section data at 30 eV. The apparent excitation cross sections and the cascade cross sections exhibit the same pressure dependence, and, when the latter is subtracted from the former, the resulting direct cross sections are independent of the pressure. Similar results are found at 50 eV, as can be seen in Fig. 6.

To determine the direct excitation cross sections at other energies, we measure the emission cross sections for transitions out of and into the $2p$ levels at a pressure of 1.0 m Torr. The resulting apparent, cascade, and direct excitation cross sections from threshold to 150 eV are summarized in Fig. 7. While the apparent excitation cross sections are expected to be larger at higher pressure, the direct excitation cross sections should be independent of the pressure.

A breakdown of the uncertainty in the measurements is as follows: For a transition in the visible-ultraviolet region, the total uncertainty is dominated by the absolute calibration procedure which is equal to 12–14% of the cross-section value. The statistical uncertainty amounts to 5% and an additional 5% is due to the measurement of the beam current and pressure. For a transition in the infrared, there is an additional uncertainty introduced due to the cross calibration of the relative FTS results. For the $In_xGa_{1-x}As$ detector, this amounts to an additional 6%, while the InSb detectors require two cross calibrations (PMT→$In_xGa_{1-x}As$→InSb) thus a somewhat higher uncertainty. The uncertainties presented in this report (Tables I and III and Figs. 5–7) reflect the total uncertainty in the cross section, including the systematic, statistical, and calibration transfer uncertainties.

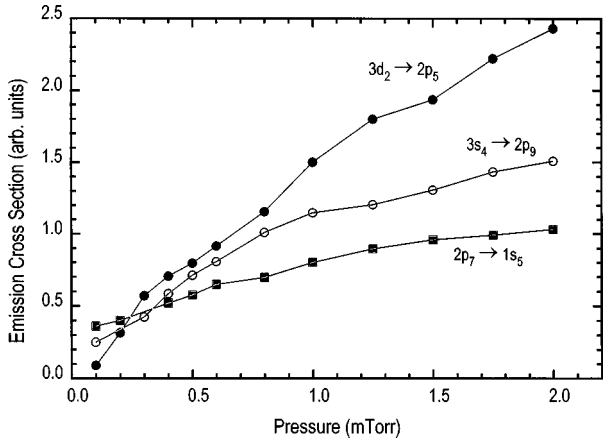

FIG. 4. Pressure dependence for the measured emission cross sections for three transitions. The three curves are normalized differently.

IV. DISCUSSION

A. Pressure dependence of the apparent excitation cross sections and the effects of cascade

Figures 5 and 6 clearly demonstrate that the variation of the apparent excitation cross sections for the $2p$ levels is entirely due to cascade. The direct excitation cross sections are independent of the pressure, and there is no evidence of appreciable contribution from collisional excitation transfer at pressures below 2.0 mTorr.

As explained in Ref. [7], the source of pressure dependence in the cascade cross sections is radiation trapping. This process is shown in Fig. 8, and has been discussed in the literature [11]. Consider two atoms initially in the ground state. Let us assume that one atom, A, undergoes a collision with an electron and is raised into an excited state k. Let us also assume that the excited state is optically connected to ground state (g) as well as some lower-lying level, i. If atom A undergoes the $k \rightarrow i$ transition, the detection of the emitted radiation will be included in the measurement of that emission cross section. If atom A undergoes the $j \rightarrow g$ transition, there is a finite probability that atom B will absorb that radiation. Upon doing so, it is now excited into level k and there is another opportunity to detect the photon corresponding to a $k \rightarrow i$ transition. Since the probability of reabsorption will increase with increasing pressure, the effective branching ratio of the $k \rightarrow i$ transition and consequently the optical emission cross section (Q_{ki}^{opt}) will increase with increasing pressure. This pressure dependence propagates to the level i through the $k \rightarrow i$ transition, making the apparent excitation cross section for level i pressure dependent even though level i is not optically connected to the ground level. This pressure dependence can further funnel down to a lower level j through the $i \rightarrow j$ radiation. In this manner the apparent excitation cross sections for all levels may acquire some pressure dependence.

The $2p$ levels are not optically connected to the ground state. Because the metastable levels $1s_3$ and $1s_5$ have very low number densities in this experiment, there should not be any significant reabsorption of the $2p \rightarrow 1s_3$ or $2p \rightarrow 1s_5$ ra-

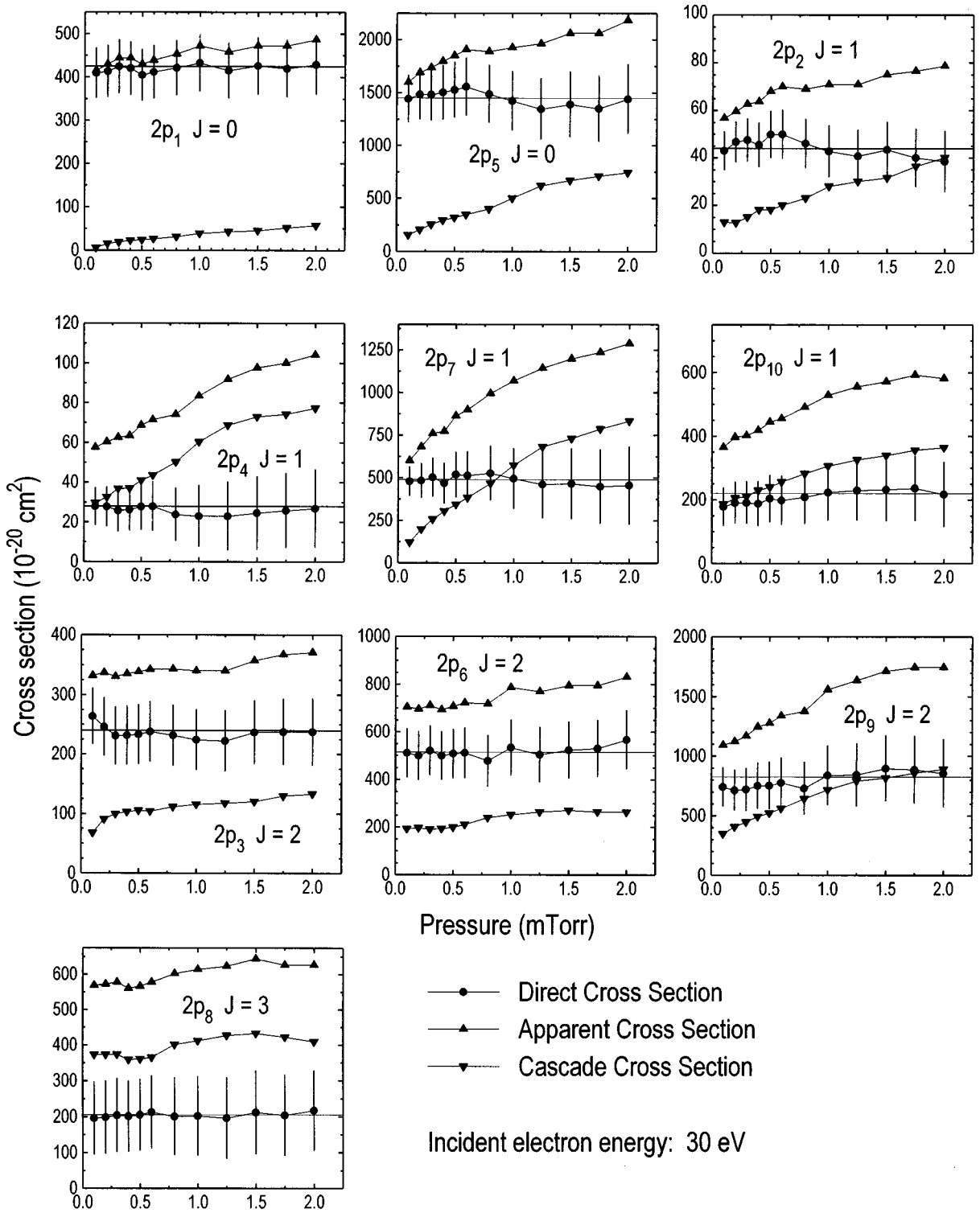

FIG. 5. Pressure dependence of the apparent, cascade, and direct cross sections for the ten $2p$ levels at an electron-beam energy of 30 eV.

diation. As a result, we would not expect to see any radiation trapping of the emissions for the transitions out of the $2p$ levels and the observed pressure dependence of the $2p$ apparent cross sections should entirely be due to cascade. In this regard, it is instructive to analyze the excitation cross-section data in light of this cascade picture, as described in the following paragraphs.

The $J=0$ levels, $2p_1$ and $2p_5$, receive cascade from only the $J=1$ levels of the s and d manifolds, which are all optically connected to the ground state. The radiation trapping associated with the cascades should result in a strong pressure dependence of the cascade portion of the apparent $2p_1$ and $2p_5$ cross sections. In Fig. 5 we find that the $2p_1$ cascade cross section increases from 6×10^{-20} to 58×10^{-20} cm^2 over the pressure range of 0.1–2.0 m Torr for an electron-beam energy of 30 eV. The apparent cross section for the $2p_1$ level increases an equivalent amount over the same pressure range. Since this increment is much

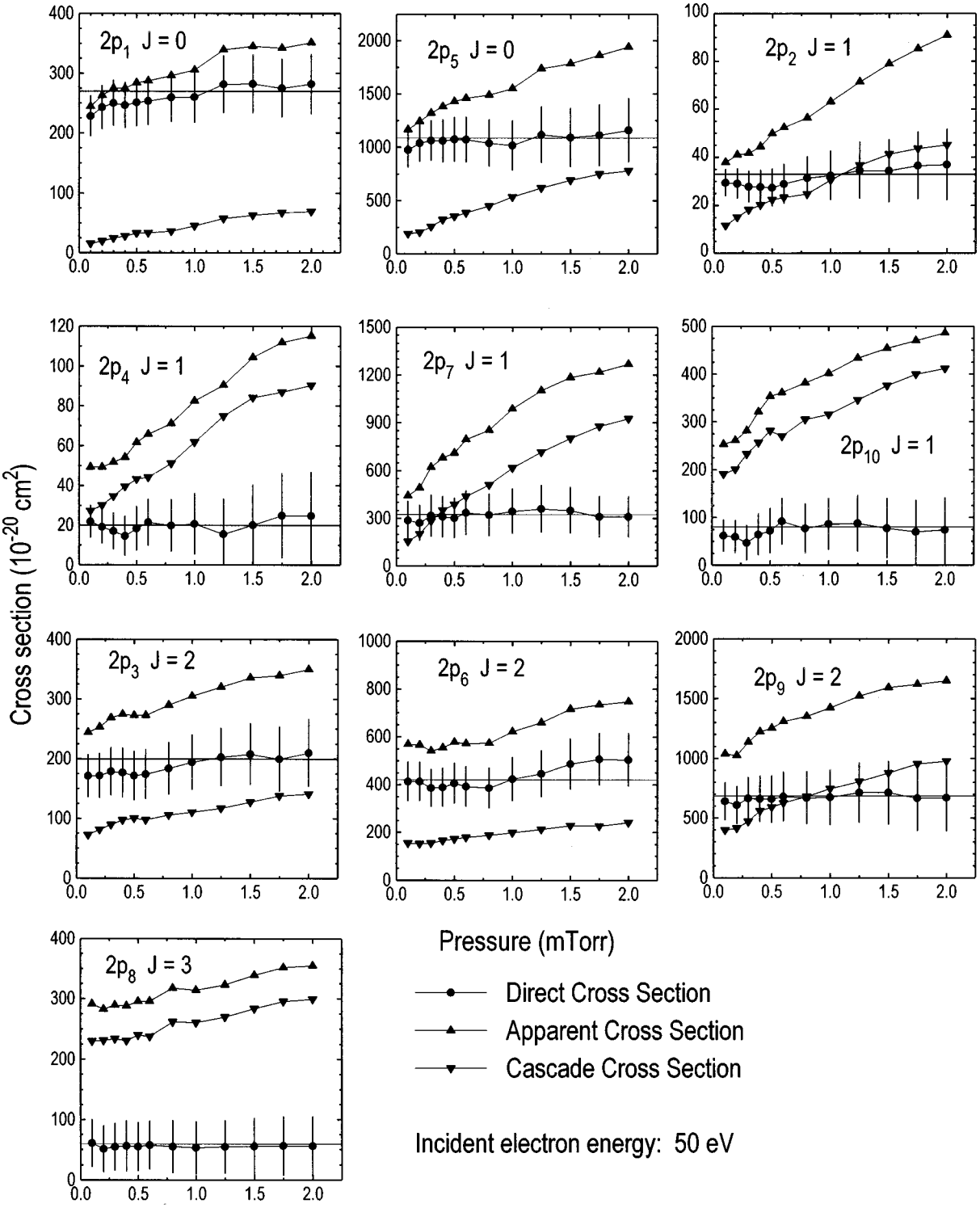

FIG. 6. Pressure dependence of the apparent, cascade, and direct cross sections for the ten $2p$ levels at an electron-beam energy of 50 eV.

smaller than the direct excitation cross section, we see only a small percentage increase in the apparent excitation cross section (Fig. 5). The $2p_5$ total cascade cross section contribution increases by more than a factor of 5, from 157 $\times 10^{-20}$ to 744$\times 10^{-20}$ cm^2, over the same pressure range. Here the cascade constitutes a much larger portion of the apparent excitation cross section. The excitation functions for optically allowed levels in general have a broader peak than those for the dipole-forbidden levels, as exemplified in Fig. 9, where the apparent excitation functions for the $4s_4$ and $4d_2$ levels (both optically allowed) are seen to be much broader than the $2p_5$ function. Since the cascade comes entirely from optically allowed transitions, the cascade cross section has a different energy dependence than the direct excitation cross section, which is evident in Fig. 7. Because of the cascade component, the excitation function for the apparent cross section falls off more slowly between 40 and 100 eV as compared to the direct excitation cross section.

The $J=1$ levels receive their cascade from the upper levels with $J=0$, 1, or 2. Of these cascading transitions, the J

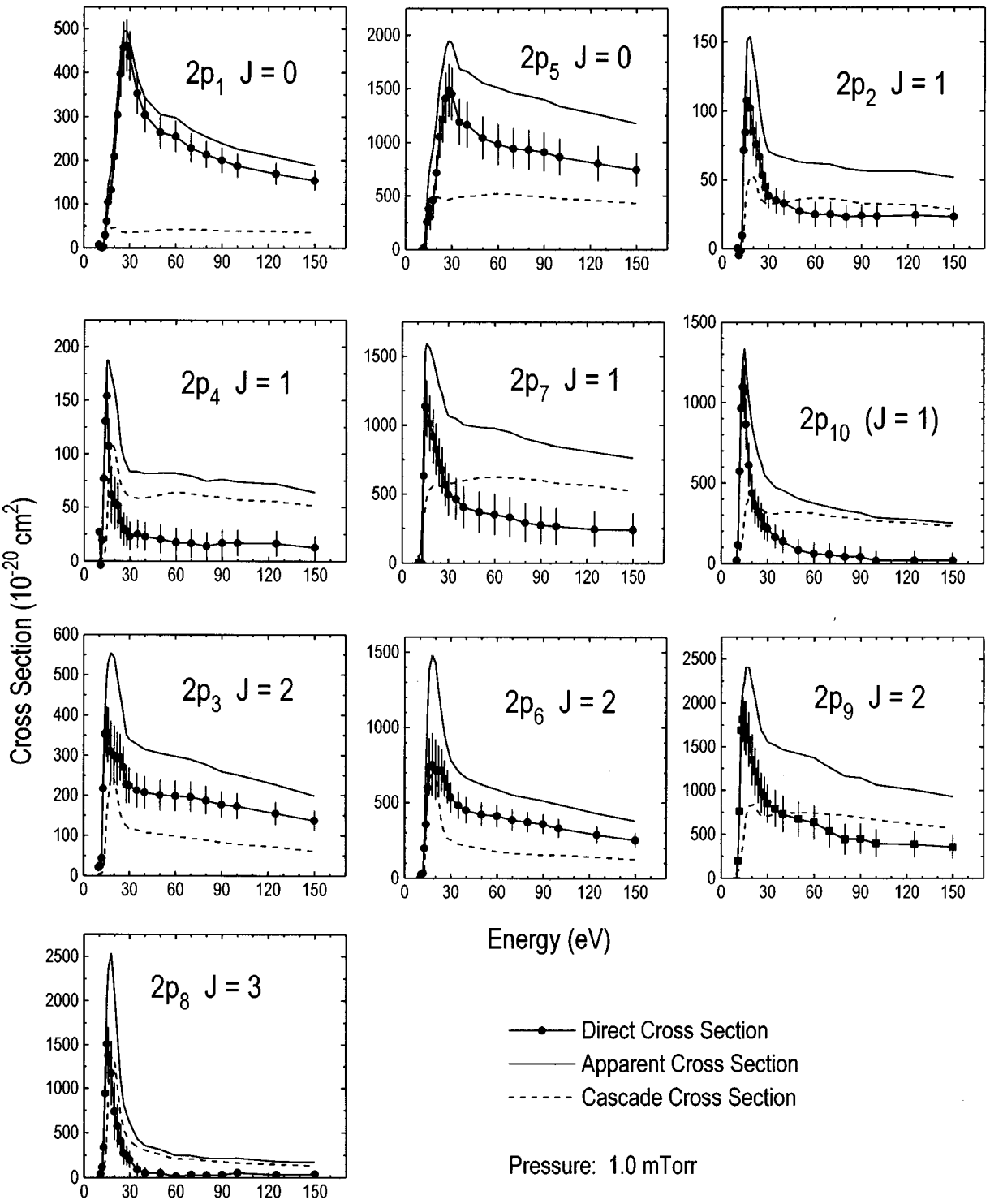

FIG. 7. Excitation functions of the apparent, cascade and direct cross sections for the ten $2p$ levels at a xenon target pressure of 1.0 m Torr.

$=0$ and 2 levels are not optically connected to the ground state so the total cascade contribution is not expected to have as strong a pressure dependence as the cascade into the $2p_1$ and $2p_5$ levels. This generalization holds for the $2p_2$, $2p_4$, and $2p_{10}$ levels. However, approximately 96% of the cascade into the $2p_7$ level at 30 eV and 1.0 m Torr comes from levels that are optically connected to the ground state, so the pressure dependence of the apparent and cascade cross sections for the $2p_7$ level is comparable to the $2p$ levels with $J=0$. In all four $J=1$ levels, the cascade causes a distortion of the excitation function because the cascade cross sections decline more slowly than the direct cross sections.

The three $J=2$ levels in the $2p$ manifold, $2p_3$, $2p_6$, and $2p_9$, receive their cascade from $J=1$, 2, and 3 levels of the s and d manifolds. Since the $2p_3$, $2p_6$, and $2p_9$, levels receive 41, 14, and 60%, respectively, from levels that are optically coupled to the ground state, at 1.0 m Torr and 30 eV, only a relatively small amount of radiation trapping is

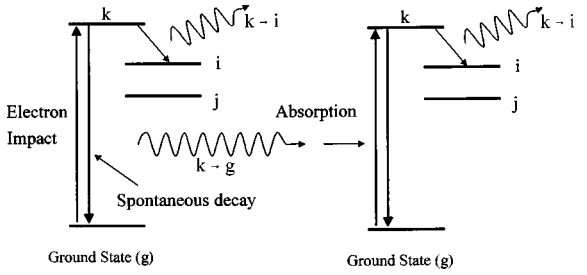

FIG. 8. Schematic diagram showing the process of radiation trapping.

expected to affect the total cascade cross sections, especially for the cases of $2p_3$ and $2p_6$. This is reflected in the relatively mild pressure dependence in the apparent excitation cross sections in Fig. 5.

The $2p_8$ level is the only level with $J=3$; it can receive cascade only from the higher lying $J=2$, 3, and 4 levels. Since none of these cascading levels are optically coupled to the ground level, pressure dependence in the apparent cross section arises only from multistep cascades. Consequently, we find a weak pressure dependence for the $2p_8$ level in Figs. 5 and 6, and much less distortion of the excitation functions (Fig. 7) than the other levels.

B. Shape of direct excitation function

An obvious feature of the direct excitation function in Fig. 8 is that the $J=3$ level ($2p_g$) exhibits the most sharply declining cross sections with increasing energy. The reason is well known, as the $2p_8$ is the only member of the $5p^5 6p$ configuration with $J=3$, and its wave function can be well approximated by a single $^3D_3$ *LS* eigenfunction. Since the ground state is a singlet state, the cross section exhibits the sharply peaked energy dependence characteristic of a spin-changing excitation. The other nine $2p$ levels have broader excitation functions because their wave functions are superpositions of singlet and triplet *LS* eigenfunctions and the singlet character in the wave function gives rise to a broader peak associated with the spin-conserving excitation. For the $2p_{10}$ level, theoretical calculations [10] show that the weighting of the singlet component is very small (2%). Thus the excitation function closely resembles that of the $2p_8$ level and is narrower than those of the other $J=1$ levels. It should be pointed out that in the case of argon, the $2p_{10}$ level also has an excitation function narrower than the other $J=1$ levels. In fact, the gross features of the direct excitation functions of Xe are generally similar to those of Ar, although the peaks for Xe are slightly narrower and occur at somewhat lower energies.

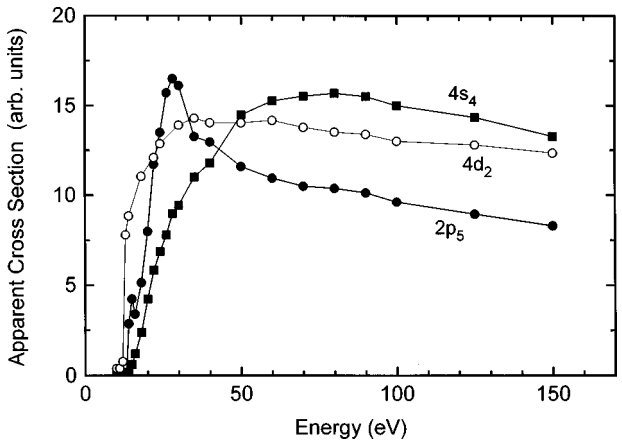

FIG. 9. Examples of the various excitation functions corresponding to excitation into levels optically coupled to the ground state ($4s_4$ and $4d_2$) as compared to the excitation functions of the $2p_5$ level. The three curves are normalized differently.

A closer examination reveals that above 30 eV the cross sections for the $J=0$ levels drop off more slowly than the other eight levels. On the other extreme is the very narrow peak of the $J=3$ level ($2p_8$). The distinction between the $J=1$ and 2 levels in this respect is not as clear, although two of the $J=1$ levels ($2p_4$ and $2p_{10}$) show a more rapid decline than all the $J=2$ levels.

For the $2p$ levels that have a substantial singlet component in their wave functions, the Born approximation predicts the cross sections to be inversely proportional to the energy at high energies, if the excitation process satisfies the selection rules for optical transitions of the electric quadrupole type [12]. On the other hand, excitation into the $2p_8$ state ($J=3$), which is a purely triplet state, is a spin-changing process. In this case the Born-Ochkur approximation predicts an E^{-3} dependence at high energies [13]. Our cross sections were measured at energies up to 150 eV, which is below the Born regime, and thus cannot be compared quantitatively with this asymptotic energy dependence. Moreover, at energies above 60 eV, the apparent and cascade cross sections for the $2p_8$ level are so close that the direct excitation cross sections obtained from their differences are subject to a large uncertainty, making a reliable comparison with the E^{-3} dependence impossible. Nevertheless, our data show that the direct excitation functions for the $2p_8$ level (a purely triplet state) and the $2p_{10}$ level (which contains very little singlet component in the wave function) fall off with energy much more rapidly than those of the other $2p$ levels, in qualitative agreement with the Born-type theory.

C. Direct excitation cross sections

Figure 7 indicates that the peak cross sections for the direct excitation into the $2p_1$, $2p_2$, $2p_3$, and $2p_4$ levels are significantly smaller than those of the other levels ($2p_5$-$2p_{10}$). This trend continues at higher energies, with the exception of the $2p_8$ and $2p_{10}$ levels, for which the cross sections decrease so rapidly with energy that they ultimately fall below the cross sections for the $2p_1$-$2p_4$ group. This sharp distinction between the $2p_1$-$2p_4$ and $2p_5$-$2p_{10}$ levels is not found in the excitation cross sections of Ar [7] and Ne [14].

In the $5p^5 6p$ configuration of Xe, the spin-orbit interaction of the $5p^5$ core is much larger than the other interactions between the $5p^5$ core and the ''outer'' $6p$ electron. A good starting approximation to describe the interaction between the core and the outer electron is to first apply l-s coupling to the $5p^5$ core (a $5p$ hole) resulting in two levels with $j_c=\frac{1}{2}$ above $j_c=\frac{3}{2}$. Each of the j_c levels is then allowed to interact with the spin and orbital angular momenta of the outer $6p$ electron ($s'=\frac{1}{2}$ and $l'=1$) so that the $j_c=\frac{1}{2}$ core level turns into a manifold of four levels ($2p_1$-$2p_4$), and the

$j_c = \frac{3}{2}$ core level into six levels ($2p_5$-$2p_{10}$). The energy spacings between the levels within each manifold are much smaller than the spacing between the two manifolds. In other words, the energy levels separate into an upper group of four ($2p_1$-$2p_4$) and lower group of six ($2p_5$-$2p_{10}$). This is indeed the pattern in Fig. 1. For the subsequent discussion, we denote a level in the $2p_5$-$2p_{10}$ group as $2p_a$ and a level in the $2p_1$-$2p_4$ group as $2p_b$.

The ionization energies of the $2p_b$ levels ($\sim$1.1 eV) are about one-half of those of the $2p_a$ levels ($\sim$2.4 eV), and this may explain the large difference in cross sections between these two groups of levels. For a hydrogen atom, the orbital radius (expectation value of r) is inversely proportional to the ionization energy. For a complex atom the ionization energy is indeed used to determine the width of the exponential wave function in the approximation of Bates and Damgaard [15]. Thus we expect a much larger orbital radius for a $2p_b$ level than a $2p_a$ level, and therefore a smaller cross section for excitation from the ground level (which has a very compact wave function) into a $2p_b$ level with a very diffusive wave function than into a $2p_a$ level. This can also be viewed from the standpoint of configuration interactions. In Fig. 1 we see that the $2p_1$-$2p_4$ levels are energetically very close to the $3p_5$-$3p_{10}$ levels. Thus the $2p_b$ level may mix significantly with the $3p$ level or even higher levels, resulting in a broadening of the extent of the $2p_b$ wave functions and consequently a reduction of the cross sections for excitation from the ground state into the $2p_b$ levels.

Next we examine individual cross sections within the $2p_a$ and the $2p_b$ groups. Here, the relation between the magnitude of the cross section and the parity of total angular momentum J is evident. In each group, the cross sections for the levels with even J are larger than those with odd J (Table III). The theoretical basis for this parity relation was discussed in the studies of electron excitation of Ne and Ar [14,16]. Neon and argon differ from xenon in that the ten $2p$ levels are quite close together and have nearly the same ionization energy (within a few percent) so that no distinction need be made on the radial extent of the wave functions for all ten levels. Consequently, the relative cross sections of the $2p$ levels are dictated primarily by the detailed coupling of the $2p^5$ (or $3p^5$) core with the outer electron, and the parity relation (the cross sections for the even-J levels being larger than the odd-J levels for the $5p^5 6p$ configuration) applies to the entire $2p$ manifold. For the case of Xe, the $2p_a$ and $2p_b$ levels have very different extents of charge distribution, which dictates the gross magnitude of the cross sections; thus the parity relation for the relative cross sections holds across only the $2p_a$ or $2p_b$ subset.

D. Comparison with previous results

The work of Fel'tsan and Zapesochnyi [1] was done over a pressure range of 0.4–1.0 mTorr, but the exact pressure at which the tabulated emission cross sections were measured was not given. Since the cross sections depend on the pressure, comparison of our data with theirs is difficult. Nevertheless, if we compare our emission cross sections taken at 1.0 m Torr with their data, we find that for most of the transitions, our results are usually larger than theirs by about 30–50% but, in some cases, such as the $2p_{10} \rightarrow 1s_5$, ours are smaller by as much as 50%. Many of our apparent cross sections, however, would be smaller if measured at 0.4 m Torr. In general, the shapes of their excitation functions are similar to our results with the exception of the $2p_7$ measurement, where they reported a second maximum (broad) at about 50 eV. Out excitation function for the $2p_7$ level shows a small shoulder forming around that energy; however, a second peak is not isolated. Another set of emission cross sections was reported by Rostovikova, Samoilov, and Smirnov [2]. Heddle and Gallagher [17] reviewed the results of Refs. [1] and [2], and pointed out that the authors of Ref. [2] used the data of Ref. [1] for calibration, yet the ratio of the corresponding peak cross section from these two sets of data ranges from 0.3 to 1.3 for the ten levels common to the two experiments.

Bogdanova and Yurgenson [18] used a pulsed electron beam to measure emissions from the $2p_1$, $2p_3$, $2p_5$, and $2p_6$ levels. The cascade population is greatly reduced if the exciting pulses of the electron beam is less than the lifetime of the cascading levels. By using the theoretical branching fractions determined from Ref. [19], Bogdanova and Yurgenson reported direct excitation cross sections for the $2p_1$, $2p_3$, $2p_5$, and $2p_6$ levels. In general, our peak direct excitation cross sections are a factor of 3–6 larger than their results, but we are unable to determine the source of this discrepancy.

As mentioned in Sec. I, DeJoseph and Clark [5] pioneered the use of FTS for detecting infrared radiation produced in electron-beam excitation experiments. They reported cross sections for transitions from the $3d$ manifold into the $2p$ manifold in the wavelength range of 1700–4000 nm, measured at a pressure of 4.0 mTorr. While the major interest of our work is focused on the excitation of the $2p$ levels, we have measured emission cross sections for the $3d \rightarrow 2p$ transitions to study the cascade into $2p$. However, we are unable to compare our $3d \rightarrow 2p$ emission cross sections with those of DeJoseph and Clark, because our measurements were made at pressures below 2.0 mTorr and the nonlinear pressure dependence makes it difficult to extrapolate our data to 4 mTorr. The shape of our $3d$ excitation functions generally agree with the results of DeJoseph and Clark, in that $3d$ levels with $J \neq 1$ show a relatively narrow peak whereas optically allowed $J = 1$ levels exhibit a much broader maximum with a small narrow peak or shoulderlike structure at a lower energy (about 20 eV).

Filipovic *et al.* [20] measured differential cross sections for a number of electronic states of Xe. By extrapolating the differential cross sections to 0° and 180° scattering angles, integral cross sections can be obtained. At 30 eV, their integral cross sections are 205×10^{-19} cm^2 for ''feature 5'' (which includes $2p_9$ and $2p_8$) and 95×10^{-19} cm^2 for ''feature 6'' (which includes $2p_7$ and $2p_6$). These are to be compared with our combined direct excitation cross sections of 108×10^{-19} cm^2 for $2p_9$ and $2p_8$ together, and of 104×10^{-19} cm^2 for $2p_7$ and $2p_6$ together, at 30 eV.

Recently Nakazaki *et al.* [21] used the *R*-matrix method to calculate direct excitation cross sections for the $2p$ levels of Xe. At 30 eV, their cross sections for the $2p_6$, $2p_7$, $2p_8$, $2p_9$, and $2p_{10}$ levels, in units of 10^{-18} cm^2, are 6.0, 4.0, 3.7, 7.6, and 4.5, respectively, in reasonable agreement with 5.4, 5.0, 2.0, 8.8, and 2.2 from our experiment.

V. CONCLUSIONS

The conventional method for detecting radiation by means of a monochromator-PMT system in an electron-beam experiment has been limited to measurements of optical cross sections for emissions in the wavelength range of about 200–1000 nm. The use of FTS for detecting infrared radiation enables us to extend this range to wavelengths as high as 2800 nm. This is of special importance for studying electron excitation of rare gases, where a large part of the emission spectrum is in the infrared. For instance, while $2p \rightarrow 1s$ emissions can be measured by a PMT system to yield the apparent excitation cross sections of the $2p$ levels, most of the strong cascade radiation into the $2p$ levels are in the infrared so that the FTS technique is needed to obtain the direct excitation cross sections. In this paper, we report optical measurements of direct excitation cross sections for the $2p$ levels of Xe using the combined capabilities of the PMT and FTS to detect the radiative transitions into and out of the $2p$ levels.

One very striking feature of the results of xenon that is *not* found in Ar or Ne is that the peak direct excitation cross sections for the $2p_1$-$2p_4$ levels are significantly smaller than those of the $2p_5$-$2p_{10}$ levels. This is explained on the grounds that the $2p_1$-$2p_4$ levels have ionization energies around 1.1 eV, which is about one-half of the ionization energies of the $2p_5$-$2p_{10}$ levels ($\sim$2.4 eV). Consequently, the wave functions for the $2p_1$-$2p_4$ levels spread out over a much wider range than do the $2p_5$-$2p_{10}$ wave functions. Thus excitation from the ground state of a very compact wave function into the highly diffusive wave function of the $2p_1$-$2p_4$ levels is less likely than excitation into the $2p_5$-$2p_{10}$ states which have a less diffuse wave function. In contrast, for the case of Ar (and also Ne), all ten $2p$ levels have nearly the same ionization energy within a few percent, and do not show markedly different peak excitation cross sections.

As far as the excitation cross sections are concerned, the $2p$ manifold of Xe ($5p^5 6p$ configuration) is separated into two subconfigurations of $2p_1$-$2p_4$ and $2p_5$-$2p_{10}$. Within each $2p$ subconfiguration the levels of even J have larger cross sections than those with odd J. This parity relation holds for the entire $2p$ manifold for Ar and Ne, but its application to Xe is limited to each subconfiguration separately because of the large differences in the spatial extent of the wave functions, as explained above.

The very drastic pressure dependence of the $2p \rightarrow 1s$ optical emission cross sections has been very puzzling for many years, ever since it was reported by Walker [3] and subsequently confirmed in other laboratories [4,5]. Our measurements of cascade radiation by means of FTS revealed the same pressure dependence for the total cascading cross sections as for the emission cross section. When the total cascades are subtracted from the apparent excitation cross sections, the resulting direct excitation cross sections are found to be independent of the pressure within experimental uncertainty. Thus the observed pressure dependence of the measured $2p \rightarrow 1s$ emission cross sections is entirely due to a cascade from the higher levels rather than to collisional excitation transfer. Radiation trapping causes the branching fraction for a transition from an optically allowed level into a lower level (other than the ground level) to increase with pressure. This results in a pressure-dependent cascade cross section, and this pressure dependence propagates to other levels through further emission.

ACKNOWLEDGMENTS

The authors wish to thank Dr. Charles A. DeJoseph for his advice on the FTS technique, which makes it possible for us to undertake this research project. Analysis of the cross sections was greatly facilitated by the theoretical transition probabilities provided by Dr. Sunggi Chung. We also wish to thank J. E. Chilton and Paul Rugheimer for their efforts in measuring many of the emission cross sections. This work was supported by the U.S. Department of Commerce, The National Institute of Standards and Technology, and by the U.S. Air force Office of Scientific Research.

[1] P. V. Fel'tsan and I. P. Zapesochnyi, Ukr. Fiz. Zh. **13**, 205 (1968) [Ukr. Phys. J. **13**, 143 (1968)].

[2] G. S. Rostovikova, V. P. Samoilov, and Yu M. Smirnov, Opt. Spektrosk. **34**, 7 (1973) [Opt. Spectrosc. **34**, 3 (1973)].

[3] K. G. Walker, Bull. Am. Phys. Soc. **29**, 158 (1984).

[4] J. E. Gastineau, C. C. Lin, L. W. Anderson, and K. G. Walker, Bull. Am. Phys. Soc. **32**, 1156 (1987).

[5] C. A. DeJoseph, Jr. and J. D. Clark, J. Phys. B **23**, 1879 (1990); and private communication.

[6] D. W. O. Heddle and C. B. Lucas, Proc. R. Soc. London, Ser. A **271**, 129 (1963).

[7] J. E. Chilton, J. B. Boffard, R. S. Schappe, and C. C. Lin, Phys. Rev. A **57**, 267 (1998).

[8] A. R. Filippelli, C. C. Lin, L. W. Anderson, and J. W. McConkey, Adv. At., Mol., Opt. Phys. **33**, 1 (1994).

[9] A. R. Filippelli, S. Chung, and C. C. Lin, Phys. Rev. A **29**, 1709 (1984).

[10] S. Chung (private communication). For the treatment of intermediate coupling, see R. D. Cowan and K. L. Andrew, J. Opt. Soc. Am. **55**, 502 (1965).

[11] See, for example, D. W. O. Heddle and M. J. Samuel, J. Phys. B **3**, 1593 (1970).

[12] See, for example, B. L. Moiseiwitsch and S. J. Smith, Rev. Mod. Phys. **40**, 238 (1968).

[13] V. I. Ochkur, Zh. Eksp. Teor. Fiz. **45**, 734 (1963) [Sov. Phys. JETP **18**, 503 (1964)].

[14] F. A. Sharpton, R. M. St. John, C. C. Lin, and F. E. Fajen, Phys. Rev. A **2**, 1305 (1970).

[15] D. R. Bates and A. Damgaard, Philos. Trans. R. Soc. London Ser. A **242**, 101 (1949).

[16] J. K. Ballou, C. C. Lin, and F. E. Fajen, Phys. Rev. A **8**, 1797 (1973).

[17] D. W. O. Heddle and J. W. Gallagher, Rev. Mod. Phys. **61**, 221 (1989).

[18] I. P. Bogdanova and S. V. Yurgenson, Opt. Spectrosk, **70**, 486 (1991) [Opt. Spectrosc. **70**, 285 (1991)].
[19] M. Aymar and M. Coulombe, At. Data Nucl. Data Tables **21**, 537 (1978).
[20] D. Filipovic, B. Marinkovic, V. Pojcev, and L. Vuskovic, Phys. Rev. A **37**, 356 (1988).
[21] S. Nakazaki, K. A. Berrington, W. B. Eissner, and Y. Itikawa, J. Phys. B **30**, 5805 (1997).